J Mater Sci (2010) 45:533–545
DOI 10.1007/s10853-009-3971-0

Crystallographic evaluation of sodium zirconium phosphate as a host structure for immobilization of cesium

Rashmi Chourasia · Ashish Bohre · Ritu D. Ambastha · O. P. Shrivastava · P. K. Wattal

Received: 5 July 2009 / Accepted: 8 October 2009 / Published online: 23 October 2009
© Springer Science+Business Media, LLC 2009

Abstract Sodium zirconium phosphate (NZP) is a potential material for immobilization of nuclear effluents. The existence of cesium containing NZP structure was determined on the basis of crystal data of solid solution. It was found that up to ~9.0 wt% of cesium could be loaded into NZP formulations without significant changes of the three-dimensional framework structure. The crystal chemistry of $Na_{1-x}Cs_xZr_2P_3O_{12}$ ($x = 0.1$–0.4) has been investigated using General Structure Analysis System programming. The CsNZP phases crystallize in the space group R-3c and $Z = 6$. Powder diffraction data have been subjected to Rietveld refinement to arrive at a satisfactory structural convergence of R-factors. The unit cell volume and polyhedral (ZrO_6 and PO_4) distortion increase with rise in the mole% of Cs^+ in the NZP matrix. The PO_4 stretching and bending vibrations in the infrared region have been assigned. SEM, TEM, and EDAX analysis provide analytical evidence of cesium in the matrix.

Introduction

The disposal of high level radioactive waste generated during reprocessing of spent fuel from nuclear reactors to recover actinides is a research problem of interest to nuclear scientists. Chemically and radiologically, reprocessed wastes are extremely complex in nature [1]. They contain fission products, residual actinides, cations from dissolution of fuel rod containers, alkali salts, and a variety of organic compounds. To reduce their volume and to stabilize their chemistry, reprocessed commercial wastes in liquid form are often converted into solid form by drying and calcining them at temperatures below 600 °C. During calcination, the wastes decompose into amorphous mixtures of chemically inert oxides while volatile reaction products are driven off. The solid products or calcines are characterized by moderate to high leachability and need to be converted to chemically stable form before they are finally disposed off. As a result, the development of waste forms that are suitable for immobilization of reprocessed high level calcines has continued to remain a challenging task for chemists. In response to this challenge, variety of waste forms including non-crystalline borosilicate glasses, crystalline, and multiphase materials has been proposed. One of them is the sodium zirconium phosphate (NZP) which allows accommodation of cations of various size and oxidation states on three distinct crystallographic sites, in fact all chemical species associated with reprocessed commercial high level waste calcines may be crystallochemically accommodated in NZP matrix [2]. Cursory studies indicate that the NZP waste forms are highly resistant to radiation damage. As crystalline waste forms, NZP compounds offer inherently low leach rate for single phases, negligible thermal expansion, and ability to immobilize high concentration of waste in high density phases. These characteristics of waste forms render these materials promising candidate for disposal of nuclear effluents. Being high-density crystalline material, it offers a notable economic advantage over less dense and thermodynamically unstable borosilicate-based glasses.

The NZP structure is a three-dimensional network of interconnected ZrO_6 octahedra and PO_4 tetrahedra, which

R. Chourasia · A. Bohre · O. P. Shrivastava (✉)
Department of Chemistry, Dr H.S. Gour University, Sagar, Madhya Pradesh 470003, India
e-mail: dr_ops11@rediffmail.com

R. D. Ambastha · P. K. Wattal
Nuclear Recycle Group, Back End Technology Development Division, B.A.R.C, Mumbai 400085, India

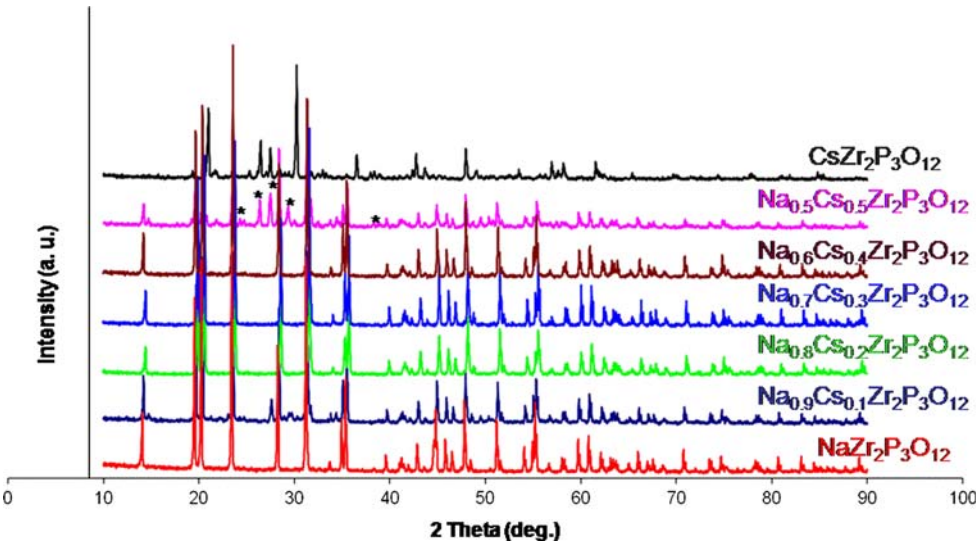

Fig. 1 Powder XRD pattern of $Na_{1-x}Cs_xZr_2P_3O_{12}$ ($x = 0.1$–1.0) ceramic samples. *Asterisk* marked peaks are due to $CsZr_2P_3O_{12}$

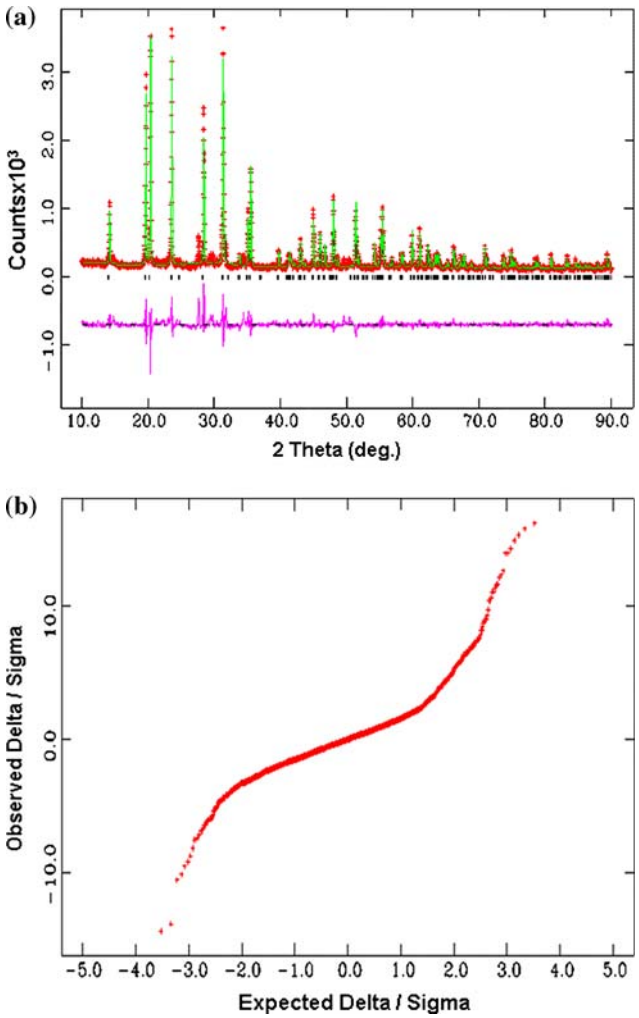

Fig. 2 **a** Rietveld refinement plot for $Na_{0.9}Cs_{0.1}Zr_2P_3O_{12}$ ceramic sample showing observed (+), calculated (*continuous line*), and difference (*lower*) curves. The *vertical bars* denote Bragg reflections of the crystalline phases. **b** Probability plot between observed intensity (I_o) and calculated intensity (I_c) for $Na_{0.9}Cs_{0.1}Zr_2P_3O_{12}$ ceramic sample

accommodates cesium ions in large interstitial cavities occupied by sodium ions in the parent structure. Fission products and other actinides substitute for zirconium as essential constituents of the three-dimensional network. In this context, several authors have reported their findings on various routes of synthesis and scientific data on

Table 1 Crystallographic data for $Na_{1-x}Cs_xZr_2P_3O_{12}$ ($x = 0.1$–0.4) phases

Structure			Rhombohedral
Space group			*R*-3*c*
Z			6
$\alpha = \beta$			90°
γ			120.0°
Parameters	$X = 0.1$	$X = 0.2$	$X = 0.4$
Lattice constants			
$a = b$	8.80623(10)	8.80841(10)	8.80997(9)
c	22.7551(4)	22.7544(5)	22.7540(5)
R_p	0.1037	0.0969	0.1071
R_{wp}	0.1391	0.1247	0.1400
$R_{expected}$	0.0673	0.0709	0.0673
RF^2	0.14074	0.12209	0.14660
Volume of unit cell	1528.230(30)	1528.943(30)	1529.454(31)
S (GoF)	2.07	1.76	2.09
D_{Wd}	0.521	0.729	0.534
Unit cell formula weight	3007.989	3073.938	3205.836
$Density_{X\text{-}ray}$	3.268	3.339	3.481
Slope	1.6887	1.4475	1.5733

$R_P = \frac{\sum y_i(o)-y_i(c)}{\sum y_i(o)}$ $R_{wp} = \left\{\frac{\sum w_i(y_i(o)-y_i(c))^2}{\sum w_i(y_i(o))^2}\right\}^2$ $R_{expected} = [(N-P)/\sum w_i y_{oi}^2]^{1/2} S = R_{wp}/R_{expected}$, where $y_i(o)$ and $y_i(c)$ are observed and calculated intensities at profile point i, respectively. w_i is a weight for each step i. N is the number of parameters refined

Table 2 Refined atomic coordinates of $Na_{1-x}Cs_xZr_2P_3O_{12}$ polycrystalline solid solutions at room temperature

Atom	x	y	z	Occupancy	$U_{isothermal}$ (Å^2)
$Na_{0.9}Cs_{0.1}Zr_2P_3O_{12}$					
Na	0.0	0.0	0.0	0.9	0.18355
Cs	0.0	0.0	0.0	0.1	0.18355
Zr	0.0	0.0	0.14577	1.0	0.05387
P	0.29175	0.0	0.25	1.0	0.0517
O_1	0.17594	−0.02524	0.19628	1.0	0.05803
O_2	0.1925	0.1742	0.08889	1.0	0.05803
$Na_{0.8}Cs_{0.2}Zr_2P_3O_{12}$					
Na	0.0	0.0	0.0	0.8	0.24108
Cs	0.0	0.0	0.0	0.2	0.24108
Zr	0.0	0.0	0.14569	1.0	0.04377
P	0.29347	0.0	0.25	1.0	0.04037
O_1	0.17594	−0.02524	0.19628	1.0	0.04848
O_2	0.194	0.17051	0.08888	1.0	0.04848
$Na_{0.6}Cs_{0.4}Zr_2P_3O_{12}$					
Na	0.0	0.0	0.0	0.6	0.8
Cs	0.0	0.0	0.0	0.4	0.8
Zr	0.0	0.0	0.14595	1.0	0.03056
P	0.29437	0.0	0.25	1.0	0.02245
O_1	0.17594	−0.02524	0.19628	1.0	0.03061
O_2	0.194	0.17051	0.08888	1.0	0.03061

corresponding simulated, mono, and multielement waste forms [3–7].

Radionuclides like ^{135}Cs and ^{129}I exhibit a half-life greater than one million years [8] and could remain harmful even after their conditioning and disposal into a geological repository. In case of groundwater contamination, iodine and cesium are believed to be the first radionuclides to reach the biosphere due to their high mobility; therefore, they have to be efficiently immobilized [9]. Besides identifying the limit of cesium loading, present communication demonstrates the scientific feasibility of cesium immobilization in the NZP matrix through an acceptable structure model based on the refinement of

Table 3 Interatomic distances (Å), polyhedral distortion, and bond valency variation of polycrystalline $Na_{1-x}Cs_xZr_2P_3O_{12}$ ceramic phases

	$X = 0.1$	$X = 0.2$	$X = 0.4$
M–O bond length			
Zr–O_1	2.031160(20)*3	2.029960(20)*3	2.026820(20)*3
Zr–O_2	2.066970(20)*3	2.068930(20)*3	2.072870(20)*3
P–O_1	1.535260(20)*2	1.544400(20)*2	1.549240(20)*2
P–O_2	1.535260(20)*2	1.516770(20)*2	1.512540(20)*2
Na_1–O_2	2.588130(30)*6	2.588340(30)*6	2.58849(4)*6
Bond length distortion (Δ)			
ZrO_6 ($\Delta \times 10^5$)	7.64	9.04	12.69
PO_4 ($\Delta \times 10^5$)	1.70	12.5	22.00
Bond valences (V_i)			
Na_1	0.808	0.807	0.806
Zr	4.45	4.44	4.45
P	5.06	5.13	5.14

$\Delta = 1/n\ \Sigma\{(R_i - R_m)/(R_m)\}2$ where R_i individual bond length, R_m average bond length, and n number of coordinations

$V_i = R_{b_{ij}}$, where $b_{ij} = (R_o/R)N$, where R is the bond length, N and R_o are constants ($N = 4.29$ and R_o is the value of the bond length for unit bond valence)

Table 4 Interatomic bond angles of polycrystalline $Na_{1-x}Cs_xZr_2P_3O_{12}$ ceramic phases

O–M–O bond angles	$X = 0.1$	$X = 0.2$	$X = 0.4$
O_2–Na_1–O_2	65.4194(10)*6	65.4319(10)*6	65.4407(11)*6
O_2–Na_1–O_2	180.0*2,179.972	179.9802*3	180.0*3
O_2–Na_1–O_2	114.5805(10)*6	114.5680(10)*6	114.5593(11)*6
O_1–Zr–O_1	90.9147(8)*3	91.0126(9)*3	91.2143(9)*3
O_1–Zr–O_2	92.0294(9)*3	92.0133(9)*3	91.9933(9)*3
O_1–Zr–O_2	175.9912(10)*3	175.8709(10)*3	175.6041(10)*3
O_1–Zr–O_2	91.7580(9)*3	91.7419(9)*3	91.7220(9)*3
O_2–Zr–O_2	85.1627(9)*3	85.0888(9)*3	84.9077(10)*3
O_1–P–O_1	107.4198(12)	106.4979(12)	106.0176(13)
O_1–P–O_2	107.69190(10)*2	107.67140(10)*2	107.65570(10)*2
O_1–P–O_2	112.1037(5)*2	112.0872(5)*2	112.0743(5)*2
O_2–P–O_2	109.8566	110.7943	111.2886

Table 5 Selected *h*, *k*, *l* values, *d*-spacing, observed, and calculated structure factors and intensity of $Na_{1-x}Cs_xZr_2P_3O_{12}$ ceramic phases

h	*k*	*l*	*d*-Space	F^2 (Obs.)	F^2 (Calc.)	Intensity (%)
$Na_{0.9}Cs_{0.1}Zr_2P_3O_{12}$						
1	0	−2	6.33490	7.648E+04	5.588E+04	27.3969
1	0	−2	6.33490	7.771E+04	5.588E+04	13.8541
1	0	4	4.55991	3.561E+05	3.453E+05	69.6383
1	0	4	4.55991	3.510E+05	3.453E+05	34.1767
1	1	0	4.40311	4.752E+05	4.980E+05	87.3229
1	1	0	4.40311	4.790E+05	4.980E+05	43.8205
1	1	3	3.80800	3.506E+05	3.066E+05	100.000
1	1	3	3.80800	3.320E+05	3.066E+05	47.1497
2	0	−4	3.16745	6.899E+05	4.722E+05	72.3761
2	0	−4	3.16745	7.700E+05	4.722E+05	40.2303
1	1	6	2.87354	5.362E+05	5.105E+05	96.3977
1	1	6	2.87354	5.132E+05	5.105E+05	45.9537
2	1	1	2.85966	5.623E+04	5.730E+04	10.0324
2	1	1	2.85966	6.110E+04	5.730E+04	5.4303
2	1	4	2.57127	1.702E+05	1.292E+05	25.8461
2	1	4	2.57127	1.497E+05	1.292E+05	11.3207
3	0	0	2.54214	5.078E+05	5.113E+05	37.9112
3	0	0	2.54214	5.063E+05	5.113E+05	18.8316
2	0	8	2.27995	1.358E+05	1.058E+05	8.6737
1	1	9	2.19258	5.029E+04	5.151E+04	6.0850
3	0	−6	2.11163	1.316E+05	1.240E+05	7.5673
2	1	−8	2.02463	2.194E+05	1.841E+05	23.8654
2	1	−8	2.02463	2.178E+05	1.841E+05	11.8057
3	1	−4	1.98258	1.348E+05	1.292E+05	14.2646
3	1	−4	1.98258	1.105E+05	1.292E+05	5.8291
2	0	−10	1.95403	1.784E+05	1.906E+05	9.2688
2	2	6	1.90400	2.771E+05	2.950E+05	27.8536
2	2	6	1.90400	2.503E+05	2.950E+05	12.5415
4	0	−2	1.88038	1.351E+05	7.798E+04	6.6820
2	1	10	1.78606	2.862E+05	3.041E+05	26.5756
2	1	10	1.78606	2.562E+05	3.041E+05	11.8588
3	1	8	1.69732	1.042E+05	1.181E+05	9.0992
3	1	8	1.69732	1.183E+05	1.181E+05	5.1525
3	2	4	1.67231	1.601E+05	1.533E+05	13.7422
3	2	4	1.67231	1.592E+05	1.533E+05	6.8142
4	1	0	1.66422	3.015E+05	2.754E+05	25.7333
4	1	0	1.66422	3.066E+05	2.754E+05	13.0486
1	0	−14	1.58966	1.832E+05	1.636E+05	7.4150
3	1	−10	1.54924	1.884E+05	2.089E+05	14.8169
3	1	−10	1.54924	1.866E+05	2.089E+05	7.3189
4	1	6	1.52395	1.056E+05	9.047E+04	8.1527
4	1	−6	1.52395	1.084E+05	9.287E+04	8.3696
2	0	14	1.49520	2.348E+05	2.566E+05	8.8768
5	0	−4	1.47325	1.548E+05	1.476E+05	5.7582
3	3	0	1.46770	1.546E+05	1.456E+05	5.7264
4	0	10	1.46142	1.379E+05	1.580E+05	5.0841

Table 5 continued

h	*k*	*l*	*d*-Space	F^2 (Obs.)	F^2 (Calc.)	Intensity (%)
2	1	−14	1.41580	1.537E+05	1.212E+05	10.9528
5	1	4	1.33169	1.435E+05	1.320E+05	9.5789
3	1	14	1.28880	8.126E+04	8.763E+04	5.2435
6	0	0	1.27107	2.331E+05	2.137E+05	7.4156
3	2	−14	1.19081	1.138E+05	9.223E+04	6.7736
4	3	10	1.09812	1.212E+05	9.376E+04	6.6449
$Na_{0.8}Cs_{0.2}Zr_2P_3O_{12}$						
1	0	−2	6.33593	4.982E+04	3.504E+04	17.4866
1	0	−2	6.33593	4.763E+04	3.504E+04	8.3212
1	0	4	4.56023	3.136E+05	2.904E+05	61.9751
1	0	4	4.56023	3.127E+05	2.904E+05	30.7736
1	1	0	4.40421	4.028E+05	4.749E+05	75.1477
1	1	0	4.40421	3.962E+05	4.749E+05	36.8054
1	1	3	3.80868	3.104E+05	2.811E+05	91.6864
1	1	3	3.80868	3.073E+05	2.811E+05	45.2171
2	0	−4	3.16797	4.857E+05	4.151E+05	54.4210
2	0	−4	3.16797	4.921E+05	4.151E+05	27.4741
1	1	6	2.87380	5.112E+05	5.018E+05	100.00
1	1	6	2.87380	5.101E+05	5.018E+05	49.7227
2	1	1	2.86036	5.286E+04	5.053E+04	10.2737
2	1	1	2.86036	6.144E+04	5.053E+04	5.9514
2	1	4	2.57176	1.602E+05	1.162E+05	27.0907
2	1	4	2.57176	1.666E+05	1.162E+05	14.0431
3	0	0	2.54277	5.179E+05	4.881E+05	43.1605
3	0	0	2.54277	5.710E+05	4.881E+05	23.7172
2	0	8	2.28011	1.105E+05	1.029E+05	8.0661
1	1	9	2.19266	5.032E+04	5.225E+04	7.0206
3	0	−6	2.11198	1.537E+05	1.163E+05	10.2804
2	1	−8	2.02485	2.138E+05	1.785E+05	27.2996
2	1	−8	2.02485	2.134E+05	1.785E+05	13.5862
3	1	−4	1.98300	1.373E+05	1.289E+05	17.1374
3	1	−4	1.98300	1.272E+05	1.289E+05	7.9181
2	0	−10	1.95412	1.781E+05	1.991E+05	10.9494
2	0	−10	1.95412	1.700E+05	1.991E+05	5.2118
2	2	6	1.90434	3.293E+05	2.903E+05	39.4031
2	2	6	1.90434	3.012E+05	2.903E+05	17.9721
4	0	−2	1.88084	8.916E+04	7.653E+04	5.2657
2	1	10	1.78619	2.864E+05	3.208E+05	32.1070
2	1	10	1.78619	2.776E+05	3.208E+05	15.5219
3	1	−7	1.77321	5.482E+04	5.460E+04	6.1005
3	1	8	1.69757	1.161E+05	1.142E+05	12.3738
3	1	8	1.69757	1.058E+05	1.142E+05	5.6286
3	2	4	1.67269	1.602E+05	1.587E+05	16.8376
3	2	4	1.67269	1.559E+05	1.587E+05	8.1714
4	1	0	1.66463	2.630E+05	2.663E+05	27.5084
4	1	0	1.66463	2.903E+05	2.663E+05	15.1502
1	0	−14	1.58963	1.620E+05	1.719E+05	8.1099

Table 5 continued

h	*k*	*l*	*d*-Space	F^2 (Obs.)	F^2 (Calc.)	Intensity (%)
4	0	−8	1.58398	1.039E+05	1.062E+05	5.1854
3	1	−10	1.54943	1.854E+05	2.267E+05	18.1254
3	1	−10	1.54943	1.772E+05	2.267E+05	8.6433
4	1	−6	1.52426	1.171E+05	9.694E+04	11.2723
4	1	6	1.52426	1.140E+05	9.444E+04	10.9814
4	1	−6	1.52426	1.082E+05	9.694E+04	5.1996
4	1	6	1.52426	1.055E+05	9.444E+04	5.0669
2	0	14	1.49522	2.704E+05	2.726E+05	12.7878
2	0	14	1.49522	2.855E+05	2.726E+05	6.7368
5	0	−4	1.47359	1.532E+05	1.613E+05	7.1498
3	3	0	1.46807	1.588E+05	1.548E+05	7.3868
4	0	10	1.46162	1.361E+05	1.733E+05	6.3061
2	1	−14	1.41585	1.468E+05	1.293E+05	13.2133
2	1	−14	1.41585	1.370E+05	1.293E+05	6.1516
4	2	−4	1.39744	6.271E+04	6.644E+04	5.5779
3	2	10	1.38722	7.952E+04	8.721E+04	7.0254
5	1	4	1.33200	1.370E+05	1.469E+05	11.6684
5	1	4	1.33200	1.303E+05	1.469E+05	5.5344
3	1	14	1.28890	9.856E+04	9.754E+04	8.1475
6	0	0	1.27139	2.570E+05	2.409E+05	10.4900
6	0	0	1.27139	2.840E+05	2.409E+05	5.7842
4	2	−10	1.21778	6.910E+04	5.869E+04	5.4232
3	2	−14	1.19093	1.109E+05	1.070E+05	8.5212
5	2	6	1.16268	7.450E+04	6.218E+04	5.5988
4	3	−8	1.14750	7.674E+04	5.995E+04	5.6954
4	3	10	1.09832	1.316E+05	1.175E+05	9.3577
$Na_{0.6}Cs_{0.4}Zr_2P_3O_{12}$						
1	0	−2	6.33667	6.386E+04	4.478E+04	17.7576
1	0	−2	6.33667	6.536E+04	4.478E+04	9.0424
1	0	4	4.56046	4.962E+05	4.753E+05	71.2789
1	0	4	4.56046	4.725E+05	4.753E+05	33.7704
1	1	0	4.40498	6.138E+05	6.917E+05	82.2412
1	1	0	4.40498	6.101E+05	6.917E+05	40.6683
1	1	3	3.80917	4.999E+05	4.536E+05	100.0001
1	1	3	3.80917	5.094E+05	4.536E+05	50.6945
2	0	−4	3.16833	7.799E+05	8.133E+05	53.8274
2	0	−4	3.16833	7.676E+05	8.133E+05	26.3584
1	1	6	2.87398	7.777E+05	7.016E+05	88.1999
1	1	6	2.87398	7.731E+05	7.016E+05	43.6231
2	1	1	2.86085	9.715E+04	8.791E+04	10.9170
2	1	1	2.86085	1.021E+05	8.791E+04	5.7057
2	1	4	2.57211	2.733E+05	2.813E+05	24.7849
2	1	4	2.57211	2.800E+05	2.813E+05	12.6341
3	0	0	2.54322	9.887E+05	7.547E+05	43.8240
3	0	0	2.54322	9.952E+05	7.547E+05	21.9480
2	0	8	2.28023	1.949E+05	1.206E+05	6.9353
1	1	9	2.19273	9.439E+04	9.927E+04	6.2115

Table 5 continued

h	*k*	*l*	*d*-Space	F^2 (Obs.)	F^2 (Calc.)	Intensity (%)
3	0	−6	2.11222	2.878E+05	1.691E+05	8.7870
2	1	−8	2.02500	4.368E+05	2.774E+05	24.5161
2	1	−8	2.02500	4.086E+05	2.774E+05	11.4120
3	1	−4	1.98331	2.632E+05	3.313E+05	14.1770
3	1	−4	1.98331	2.567E+05	3.313E+05	6.8772
2	0	−10	1.95418	3.892E+05	4.820E+05	10.1762
2	0	−10	1.95418	3.893E+05	4.820E+05	5.0643
2	2	6	1.90458	7.624E+05	5.458E+05	37.8887
2	2	6	1.90458	7.204E+05	5.458E+05	17.8143
4	0	−2	1.88116	2.085E+05	2.147E+05	5.0544
2	1	10	1.78629	6.805E+05	7.926E+05	29.8058
2	1	10	1.78629	6.302E+05	7.926E+05	13.7339
3	1	8	1.69776	2.728E+05	2.177E+05	10.8215
3	2	4	1.67296	4.073E+05	4.268E+05	15.7046
3	2	4	1.67296	4.524E+05	4.268E+05	8.6805
4	1	0	1.66493	7.368E+05	5.895E+05	28.1449
4	1	0	1.66493	7.071E+05	5.895E+05	13.4407
1	0	−14	1.58962	4.455E+05	3.514E+05	7.7881
4	0	−8	1.58417	2.922E+05	2.244E+05	5.0749
3	1	−10	1.54956	4.879E+05	6.269E+05	16.2549
3	1	−10	1.54956	4.866E+05	6.269E+05	8.0688
4	1	−6	1.52448	2.811E+05	2.363E+05	9.0817
4	1	6	1.52448	2.735E+05	2.297E+05	8.8361
2	0	14	1.49524	7.110E+05	6.457E+05	11.0822
2	0	14	1.49524	7.680E+05	6.457E+05	5.9579
5	0	−4	1.47383	5.288E+05	4.853E+05	8.0263
4	0	10	1.46176	5.301E+05	5.043E+05	7.9265
3	3	0	1.46833	3.916E+05	4.097E+05	5.9031
2	1	−14	1.41589	4.387E+05	3.210E+05	12.3851
2	1	−14	1.41589	4.080E+05	3.210E+05	5.7350
4	2	−4	1.39767	2.028E+05	2.085E+05	5.5963
3	2	10	1.38736	2.141E+05	2.769E+05	5.8297
5	1	4	1.33222	4.995E+05	4.960E+05	12.6865
5	1	4	1.33222	4.936E+05	4.960E+05	6.2420
3	1	14	1.28897	2.958E+05	2.954E+05	7.1127
6	0	0	1.27161	8.983E+05	8.574E+05	10.5689
6	0	0	1.27161	9.536E+05	8.574E+05	5.5876
4	2	−10	1.21793	2.299E+05	2.237E+05	5.0646
3	2	−14	1.19102	3.850E+05	3.872E+05	8.2126
5	2	6	1.16287	2.475E+05	2.576E+05	5.1114
4	3	−8	1.14766	3.047E+05	2.467E+05	6.1854
4	3	10	1.09846	5.328E+05	5.611E+05	10.2819
4	3	10	1.09846	5.330E+05	5.611E+05	5.1304

The reflection selected from the crystallographic information framework output of the final cycle of the refinement

Intensities <5% were omitted

crystallographic data. It also investigates the crystallochemical changes due to matrix modification when a large cation like Cs^+ is substituted for sodium on M_1 site of the NZP framework.

Experimental

Ceramic route synthesis of $Na_{1-x}Cs_xZr_2P_3O_{12}$ phases

Calculated quantities of AR grade Na_2CO_3, $CsNO_3$, ZrO_2, and $(NH_4)H_2PO_4$ for the stoichiometry $Na_{1-x}Cs_xZr_2P_3O_{12}$ ($x = 0.1$, 0.2, 0.3, 0.4 0.5, and 1) were thoroughly mixed with about 10 mL of 1,2,3-propane triol to form a semi-solid paste. The glycerol paste was gradually heated initially at 600 °C for 4 h in a crucible. This initial heating is done to decompose Na_2CO_3 and $(NH_4)H_2PO_4$ with emission of carbon dioxide, ammonia, and water vapors. The mixture was reground to micron size, pressed into pellets, and sintered in a platinum crucible at 1200 °C for 12 h. The process was repeated to get a polycrystalline dense material.

Characterization

The powder X-ray diffraction (XRD) pattern has been recorded between $2\theta = 10°$ and 90° on a Pan Analytical diffractometer (XPERT-PRO) using CuKα radiation at a step size of $2\theta = 0.017°$ and a fixed counting time of 5 s/step. Scanning electron microscopy (SEM) has been carried out on an electron microscope system (HITACHI S-3400) equipped with Thermonoran ultra dry detector facility for energy dispersive X-ray (EDAX) analysis. Transmission electron microscopy (TEM) study was done with a PHILIPS CM200 analytical instrument operated between 20 and 200 kV.

Results and discussion

Rietveld refinement and crystallographic model of the phases

The powder XRD data showed that monophases of composition $Na_{1-x}Cs_xZr_2P_3O_{12}$ ($x = 0.1$–0.4) are isostructural to $NaZr_2(PO_4)_3$ but beyond $x = 0.4$ secondary phase of cesium zirconium phosphate ($CsZr_2P_3O12$) begins to appear along with NZP (Fig. 1) [10]. CsNZP crystallizes in the rhombohedral system (space group *R*-3*c*). The conditions for the rhombohedral lattice: (i) $h + k + l = 3n$, (ii) when $h = 0$, $l = 2n$, and (iii) when $k = 0$, $l = 2n$ have been verified for all reflections between $2\theta = 10°$ and 90°. The intensity and positions of the diffraction pattern match with the characteristic pattern of parent compound NZP, which gives several prominent reflections between $2\theta = 13.98°$ and 46.47° [11]. The Rietveld [12] refinement of the step scan data was performed by the least square method using General Structure Analysis System software [13]. Assuming that CsNZP belongs to the Nasicon family, Zr, P, and O atoms are in the *12c*, *18e*, and *36f* Wyckoff positions, respectively, of the *R*-3*c* space group. In CsNZP phases, the Na atoms were assumed to occupy the M_1 (*6b*) site and M_2 site (*18e*). The occupancies of Na and Cs atoms have been constrained according to their theoretical molar ratios. The structure refinement leads to rather good agreement between the experimental and calculated XRD pattern (Fig. 2a) and yields acceptable reliability factors: RF^2, R_p, and R_{wp} [14]. The normal probably plot for the histogram gives nearly a

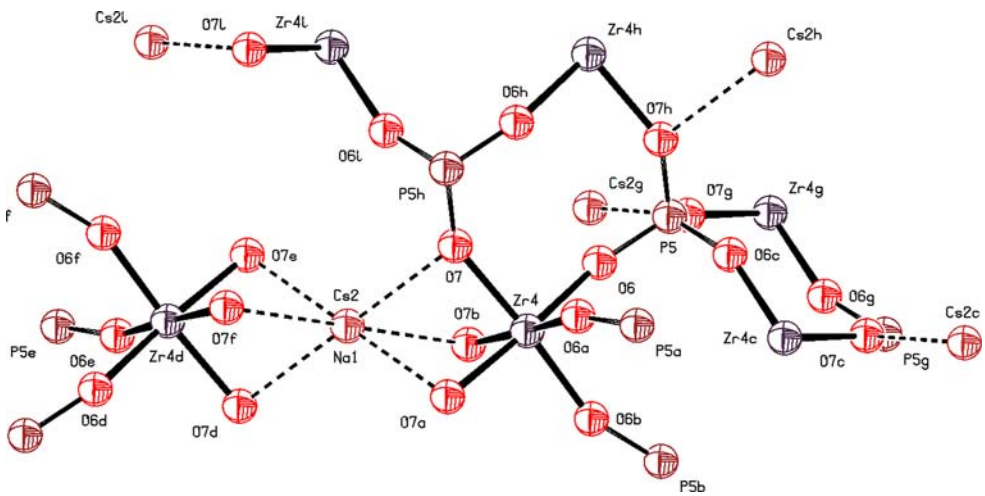

Fig. 3 PLATON view of molecular structure of $Na_{0.9}Cs_{0.1}Zr_2P_3O_{12}$ showing Zr coordination in ZrO_6 and P coordination in PO_4 polyhedron at 50% probability level

linear relationship indicating that the I_o and I_c values for the most part are normally distributed (Fig. 2b). The lattice parameters are close to the corresponding values for unsubstituted NZP unit cell [15]. The cell parameters of the specimens register slight increase in *a* direction (Table 1). Simultaneously, the structure shows a little contraction along *c* direction due to angular distortions as a result of the coupled rotation of ZrO_6 and PO_4 polyhedrons [16]. Alteration in lattice parameters shows that the network modifies its dimensions to accommodate the cations occupying M_1 site without breaking the bonds. The basic framework of NZP accepts the cations of different sizes and oxidation states to form solid solutions but at the same time retaining the overall geometry unchanged. The cell volume of the specimens registers slight increase. In this study, the observed change in lattice parameters is not significant as compared to earlier reports [17–21]. The final atomic coordinates and isotropic thermal parameters (Table 2), inter-atomic distances, polyhedral distortions along with bond valences (Table 3) and bond angles (Table 4) are extracted from the crystal information file prepared after final cycle of the refinement. Selected *h*, *k*, *l* values, *d*-spacing, and intensity data along with observed and calculated structure factors have been listed in Table 5. The refinement leads to acceptable Zr–O, P–O bond distances. Zr atoms are displaced from the center of the octahedron due

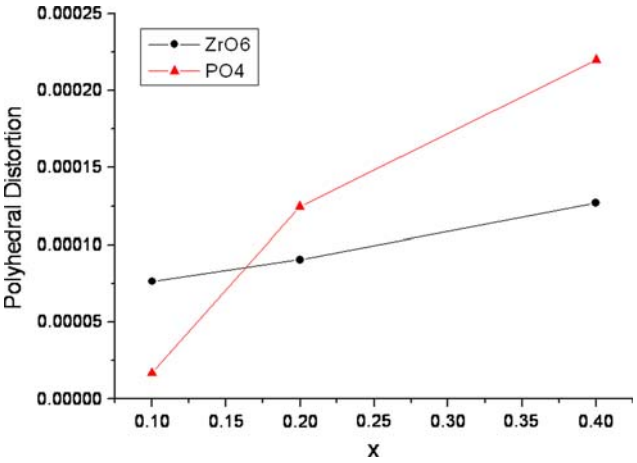

Fig. 5 Variation of polyhedral distortions in the $Na_{1-x}Cs_xZr_2P_3O_{12}$ solid solutions with cesium loading

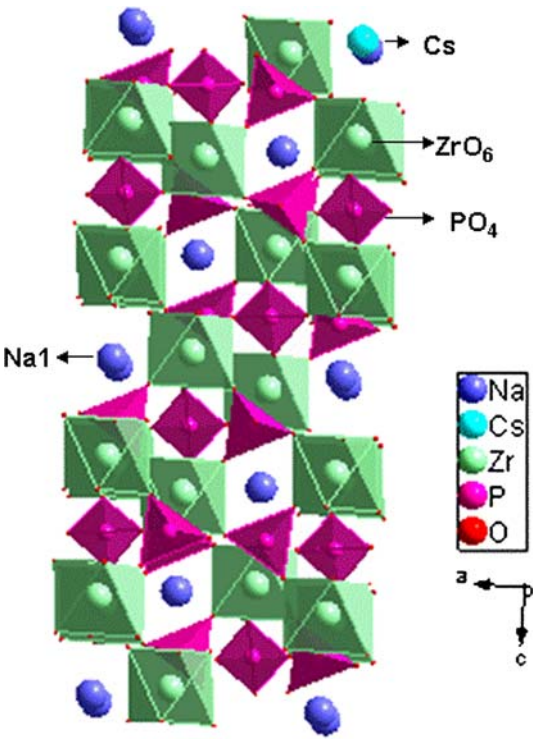

Fig. 4 DIAMOND view of crystal structure of $Na_{0.9}Cs_{0.1}Zr_2P_3O_{12}$ ceramic phase

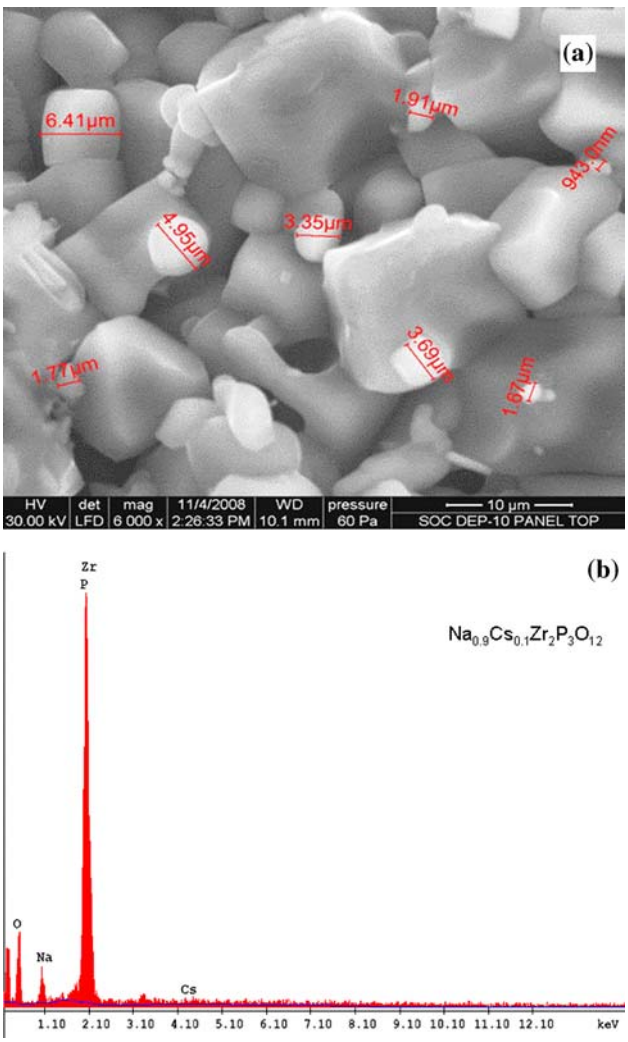

Fig. 6 **a** SEM. **b** EDAX spectrum of $Na_{1-x}Cs_xZr_2P_3O_{12}$ ($x = 0.1$) ceramic phases

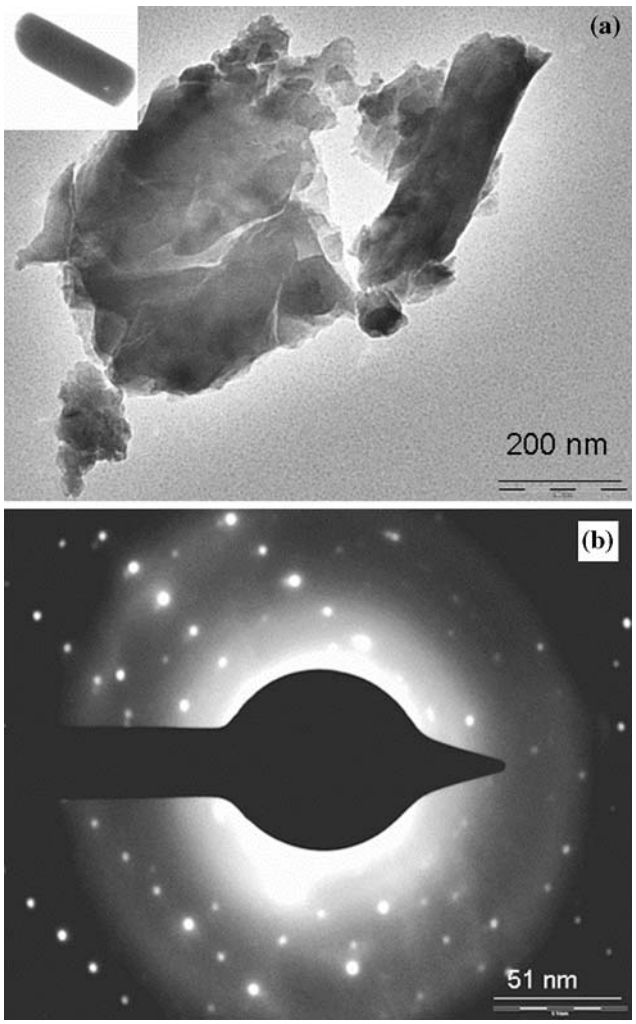

Fig. 7 **a** TEM image of the bulk nano phase and isolated crystal (*inset*) of $Na_{0.9}Cs_{0.1}Zr_2P_3O_{12}$. **b** SAED image of $Na_{0.9}Cs_{0.1}Zr_2P_3O_{12}$ polycrystalline powder showing the fundamental reflections

Table 6 Distribution of particle size (nm) along with prominent reflecting planes of $Na_{1-x}Cs_xZr_2P_3O_{12}$ ceramic sample

hkl	$X = 0.1$	$X = 0.2$	$X = 0.4$
10−2	95.84	47.90	79.83
104	80.40	80.40	80.40
110	80.50	48.30	96.67
113	69.36	69.40	69.40
20−4	81.68	61.33	61.33
211	123.43	101.24	123.51
214	124.64	49.70	124.30
300	136.45	62.37	99.82
226	106.630	85.40	106.73
2110	108.09	86.57	86.56
229	110.02	88.11	110.14
31−10	89.93	75.03	112.55

Table 7 Assignment (cm^{-1}) of IR bands for $Na_{1-x}Cs_xZr_2P_3O_{12}$ ceramic samples

Compound	υ_3 υ_{as} (P–O)	υ_1 υ_s (P–O)	υ_4 δ (P–O)	υ_2 (P–O)
$Na_{0.9}Cs_{0.1}Zr_2P_3O_{12}$	1265m, 1197m, 1109sh, 1060s	968sh, 933w	640s, 576s, 555s, 540w, 507s	470s, 443s, 418s
$Na_{0.8}Cs_{0.2}Zr_2P_3O_{12}$	1271m, 1211sh, 1153m, 1097s, 1082w, 1060sh	968sh, 939w	638s, 574s, 553s, 513s	484s, 457s, 435s
$Na_{0.7}Cs_{0.3}Zr_2P_3O_{12}$	1269s, 1211s, 1151s, 1107sh, 1060s	966sh, 949sh, 931sh, 900w	638s, 576s, 555s	482s, 459s, 443s, 405s
$Na_{0.6}Cs_{0.4}Zr_2P_3O_{12}$	1271s, 1209s, 1149sh, 1114w, 1093w, 1060s, 1022w	987sh, 979sh, 898s	640s, 576s, 555s, 513w	445s, 401s
$Na_{0.5}Cs_{0.5}Zr_2P_3O_{12}$	1201s, 1172w, 1095sh, 1087sh, 1060s	995sh	648s, 576w, 536s, 522w	486s, 443s, 418, 408
$CsZr_2P_3O_{12}$	1178m, 1051sh, 1035sh	985sh	636s, 605s, 592s, 545s, 515w	432s, 418s

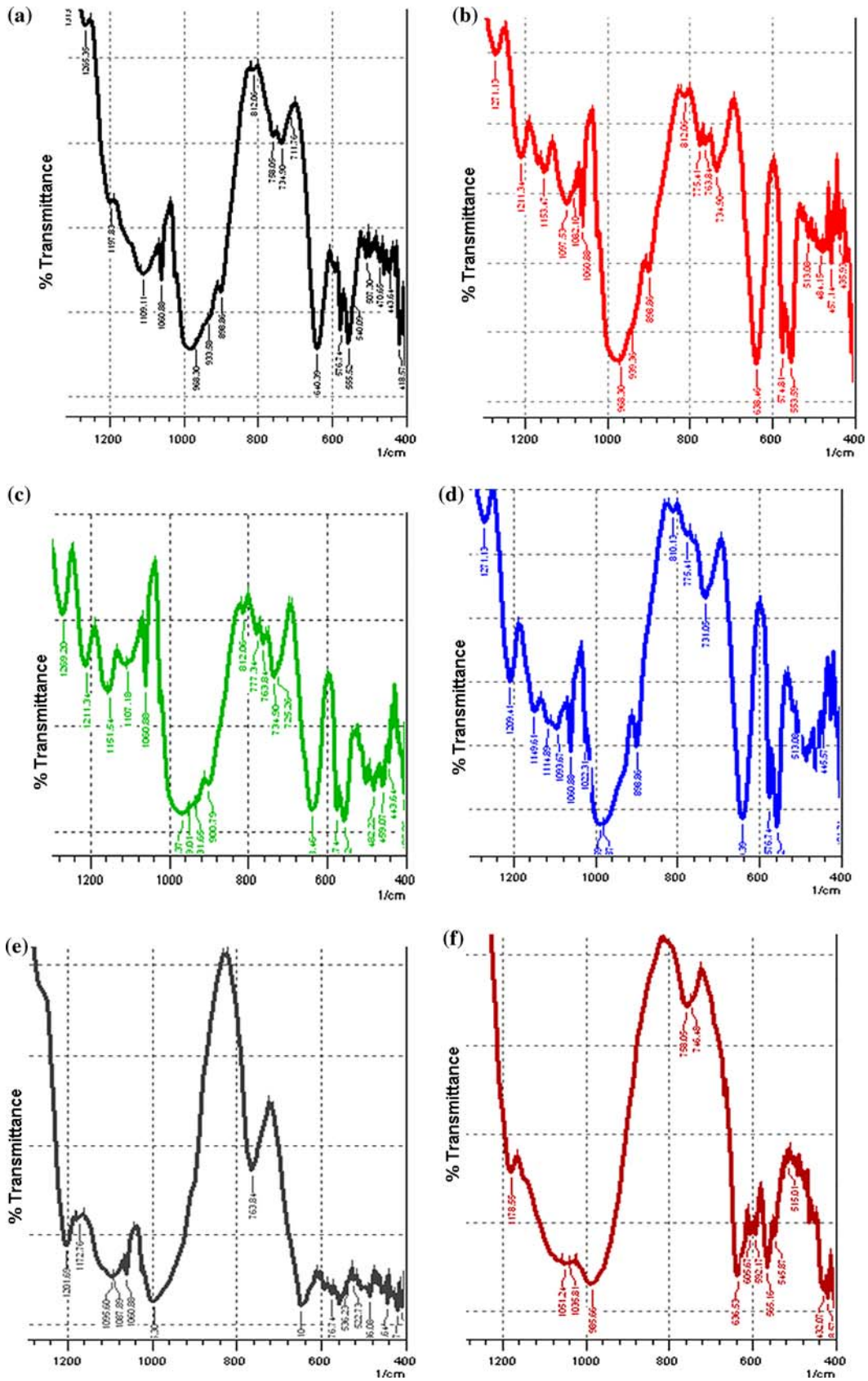

Fig. 8 IR spectra of $Na_{1-x}Cs_xZr_2P_3O_{12}$, **a** $x = 0.1$, **b** $x = 0.2$, **c** $x = 0.3$, **d** $x = 0.4$, **e** $x = 0.5$, and **f** $x = 1.0$

to the Na^{+}–Zr^{4+} repulsions. Consequently, the Zr–O(2) distance (2.067, 2.069, 2.0729 Å), neighboring the sodium Na(1), is slightly greater than the Zr–O(1) distance (2.0311, 2.0299, 2.0268 Å); however, average Zr–O distances are smaller than the values calculated from the ionic radii data (2.12 Å) [22]. The O–Zr–O angles vary between 84.90° and 175.9°. The angles implying the shortest bonds are superior to those involving the longest ones due to O–O repulsions which are stronger for O(1)–O(1) than for O(1)–O(2).

The P–O distances (in pairs) 1.536, 1.544, and 1.549 Å are close to those found in Nasicon type phosphates. The O–P–O angles vary between 106.01° and 112.10°. Figure 3 shows the PLATON projection of the molecular structure depicting the inter linking of ZrO_6 and PO_4 through a bridge oxygen atom. Figure 4 illustrates the DIAMOND view showing the ZrO_6 inter ribbon distance in the structure of the title phase which is a function of amount and size of alkali cation in the M(2) site of the 3D framework, built from ZrO_6 octahedrons and corner sharing PO_4 tetrahedrons. Substitution of Na^{+} by larger cation of Cs^{+} results in linear increase in distortion in ZrO_6 and PO_4 polyhedra (Fig. 5). Calculated valences (V_i) [23] based on bond strength analysis [24, 25] are in agreement with the expected oxidation states of Na^{+}, Zr^{4+}, and P^{5+}, respectively.

SEM and TEM analysis

Within permissible statistical limits, the weight and atomic % of Na, Cs, Zr, P, and O are agreeable with the EDAX analysis. In $Na_{0.9}Cs_{0.1}Zr_2P_3O_{12}$, the wt% ratios Cs/Na were found to be 0.66 against the calculated value of 0.64. Likewise, the observed and calculated atomic ratios in this specimen are 0.17 and 0.11, respectively. The EDAX spectra provide the evidence of cesium in the polycrystalline mono phases, whereas SEM shows the typical morphology of the grains of 0.943–2.5 μm in length (Fig. 6a, b). In TEM, the nano powder was observed in the form of non-uniform agglomerates (Fig. 7a). Simultaneously, the particle size was also determined using the Scherrer's equation where broadening of peak is expressed as full width at half-maxima in the recorded XRD pattern [26] (Table 6). The particle size varies between 48 and 137 nm. The selected area electron diffraction (SAED) pattern of nano ceramic shows concentric rings in the diffraction pattern, which confirms the polycrystalline nature of the ceramic powder. Crystallographic planes and ordered arrangement of atoms are visible in the electron microscopy image (Fig. 7b).

Infrared analysis

The presence of orthophosphate anions in the crystal structure was confirmed with the infrared (IR) spectroscopy. The absorption bands in the range between 1250–1022 cm^{-1} and 650–507 cm^{-1} are assigned to stretching and bending vibrations of P–O bonds of the PO_4 tetrahedron, respectively. The stretching vibrations occur between 1270 and 1020 cm^{-1} as υ_3 band, the symmetric stretching υ_1 and antisymmetric bending υ_4 vibrations are observed in the regions 990–900 cm^{-1} and 640–505 cm^{-1} respectively [27–29] (Table 7 and Fig. 8a–f).

Conclusions

Principally phase pure cesium containing NZP formulations can be prepared with simulated cesium loadings up to ~9 wt%, beyond these limit traces of minor secondary phase of cesium zirconium phosphate starts appearing along with the solid solution. The Rietveld plots represent a good structure fit between observed and calculated intensity with satisfactory *R*-factors. The bond distances Zr–O, P–O, Na–O are in agreement with their corresponding values for respective oxides. The bond distortions in ZrO_6 and PO_4 polyhedra vary linearly with respect to cesium loading but the overall structure of the matrix remains intact.

Acknowledgements The authors are grateful to the Department of Science and Technology (DST), New Delhi, Government of India, for funding research Project Number SR/S3/ME/20/2005-SERC-Engg in its SERC scheme. Thanks are due to sophisticated analytical instrument facility, IIT, Bombay, for TEM analysis and department of Metallurgical Engineering and Material Science IIT, Bombay, for XRD analysis.

References

1. Hawkins HT, Scheetz BE (1996) In: Proceedings of the material research society 1996, fall meeting, Boston, MA, 2–6 December
2. Pet'kov VI, Sukhanov MV (2003) Czechoslovak J Phys 53:A671
3. Hirose Y, Fukasawa T, Agrawal DK, Scheetz BE, Nageswaran R, Curtis JA, Limaye SY (1999) In: WM 1999 conference
4. Scheetz BE, Agarwal DK, Breval E, Roy R (1994) Waste Manage 14(6):489
5. Donald IW, Metcalfe BL, Taylor RNJ (1997) J Mater Sci 32:5851. doi:10.1023/A:1018646507438
6. Shrivastava OP, Chourasia R (2007) J Hazard Mater 153:285
7. Chourasia R, Shrivastava OP, Wattal PK (2009) J Alloys Compd 473(1–2):579
8. Lide DR (1992–1993) Handbook of chemistry and physics, Sect. 11, 73rd ed. CRC Press, Boca Raton, FL
9. Renaud P, Beaugelin K, Maubert H, Ledenvic P (1997) Cons′equences radiologiques et dosim′etriques de l'accident de Tchernobyl en France (Rapport IPSN 97-03, IPSN, France, 1997)
10. Rustam R, Vance ER, Alamo J (1982) Mater Res Bull 17:585
11. JCPDS Powder diffraction data file no. 71-0959 (2000) compiled by International Center for Diffraction Data, USA
12. Rietveld HM (1996) J Appl Cryst 2:65
13. Larson AC, Von Dreele RB (2000) General structure analysis system technical manual. LANSCE, MS-H805, Los Almos National Laboratory LAUR 86-748

14. Kojitani H, Kido M, Akaogi M (2005) Phys Chem Miner 32:290
15. Verissimo C, Garrido FMS, Alves OL, Calle P, Juarez AM, Iglesias JE, Rojo JM (1997) Solid State Ionics 100:127
16. Govindan Kutty KV, Asuvathraman R, Sridhran R (1998) J Mater Sci 33:4007. doi:10.1023/A:1004661132398
17. Lenain GE, McKinstry HA, Limaye SY, Woodward A (1984) Mater Res Bull 19:1451
18. Petíkov VI, Orlova AI, Kazantsev GN, Samoilov SG, Spiridonova ML (2001) J Therm Anal Calorim 66:623
19. Oota T, Yamai I (1986) J Am Ceram Soc 69(1):1
20. Lenain GE, McKinstry HA, Alamo J, Agrawal DK (1987) J Mater Sci 22:17. doi:10.1007/BF01160546
21. James A, Rustam R (1986) J Mater Sci 21:444. doi:10.1007/BF01145507
22. Shannon RD (1976) Acta Crystallogr A 32:751
23. Shrivastava OP, Chourasia R (2008) J Chem Crystallogr 38:357
24. Brown ID, Shannon RD (1973) Acta Crystallogr A29:266
25. Breese NE, Keeffe MO (1991) Acta Crystallogr B47:192
26. Shrivastava OP, Chourasia R, Kumar N (2008) Ann Nucl Energy 35–36:1147
27. Buvaneswari G, Varadaraju UV (1999) J Solid State Chem 145: 227
28. Barj M, Perthuis H, Colomban Ph (1983) Solid State Ionics 11: 157
29. Mbandza A, Bordes E, Courtine P (1985) Mater Res Bull 20:251